L450W and Q455K *Col8a2* Knock-In Mouse Models of Fuchs Endothelial Corneal Dystrophy Show Distinct Phenotypes and Evidence for Altered Autophagy

Huan Meng,[1] *Mario Matthaei,*[1,2] *Narendrakumar Ramanan,*[3] *Rhonda Grebe,*[1] *Shukti Chakravarti,*[1,4] *Caroline L. Speck,*[1] *Martha Kimos,*[1] *Neeraj Vij,*[5] *Charles G. Eberhart,*[1] *and Albert S. Jun*[1]

Purpose. We compared the cellular phenotypes and studied the role of autophagy in the pathogenesis of Fuchs endothelial corneal dystrophy (FECD) using two α2 collagen VIII (*Col8a2*) knock-in mouse models and human FECD tissues.

Methods. In vivo corneal endothelial cell (CEC) counts and morphology were analyzed by clinical confocal microscopy. Ultrastructural analysis of CECs was performed by transmission electron microscopy. Real-time PCR and Western blotting were performed using total RNA, and protein extracted from mouse CECs and human CECs obtained from FECD and autopsy patients.

Results. Both *Col8a2* mouse models exhibited hallmarks of FECD; however, the $Col8a2^{L450W/L450W}$ mice exhibited a milder phenotype compared to the $Col8a2^{Q455K/Q455K}$ mice. Both models exhibited upregulation of the unfolded protein response (UPR) as evidenced by dilated rough endoplasmic reticulum (RER), and upregulation of UPR-associated genes and proteins. Real-time PCR of $Col8a2^{L450W/L450W}$ and $Col8a2^{Q455K/Q455K}$ CECs at 40 weeks revealed a 2.1-fold ($P < 0.05$) and a 5.2-fold ($P < 0.01$) upregulation of the autophagy marker *Dram1*, respectively. Real-time PCR of human FECD endothelium revealed a 10.4-fold upregulation of *DRAM1* ($P < 0.0001$) compared to autopsy controls.

Conclusions. The $Col8a2^{L450W/L450W}$ and $Col8a2^{Q455K/Q455K}$ mouse models of FECD showed distinct endothelial cell phenotypes. *Dram1* was associated with activation of the UPR and increased autophagy. Overexpression of this gene in mouse and human FECD endothelial cells suggested a role for altered autophagy in this disease. (*Invest Ophthalmol Vis Sci.* 2013;54:1887–1897) DOI:10.1167/iovs.12-11021

Fuchs endothelial corneal dystrophy (FECD) is characterized by bilateral, progressive loss of corneal endothelial cells (CECs) across several decades. FECD affects approximately 5% of the population in the United States, with a higher frequency among Caucasian populations.[1] In 2009, FECD accounted for 23% of corneal transplants performed in the United States.[2] The definitive treatment for visually significant FECD is endothelial transplantation. No early or nonsurgical therapy to delay or prevent disease progression currently exists to our knowledge.

The hallmark pathologic features of FECD include loss of corneal endothelial cells and the presence of guttae, which are drop-like excrescences of extracellular matrix arising from the underlying Descemet membrane (DM).[3] DM is the basement membrane of the CECs, and its primary component is collagen type VIII (COL8), a nonfibrillar, short chain collagen secreted by CECs. In FECD corneas, DM becomes thickened with irregularly deposited wide-spaced COL8 aggregates.[4]

In the normal cornea, a smooth monolayer of CECs, uniform in size and shape, is present along the DM. CECs form a selective barrier to the aqueous fluid[5] with the activity of sodium-potassium ATPase and carbonic anhydrase on the apical surface maintaining physiologic hydration and clarity of the cornea. Arrested in G1 phase of the cell cycle, human CECs have very limited replicative potential in vivo.[6] Human and mouse CECs undergo physiologic decline in cell number with aging.[7–9] With severe CEC loss in FECD, significant corneal edema causes loss of visual acuity.

Studies of early disease pathogenesis in FECD largely are lacking. Genetic studies have identified multiple gene mutations and loci associated with FECD (Online Mendelian Inheritance in Man #136800, available in the public domain at http://www.ncbi.nlm.nih.gov/omim). These include missense mutations Q455K and L450W in the gene encoding the α2 subunit of collagen VIII (COL8A2) associated with an early-onset form of FECD.[10–12] Transmission electron microscopy (TEM) of corneal tissues obtained from FECD patients with unknown genotypes reveal enlarged rough endoplasmic reticulum (RER), suggestive of endoplasmic reticulum (ER) stress caused by the accumulation of misfolded proteins in the ER lumen.[13–15] Previous studies in human FECD corneal tissue[13] and a $Col8a2^{Q455K/Q455K}$ mutant mouse model of FECD[16] show activation of ER stress and the unfolded protein response (UPR).

From the [1]Wilmer Eye Institute, and the [4]Department of Medicine, Johns Hopkins Medical Institutions, Baltimore, Maryland; the [2]Department of Ophthalmology, University Medical Center Hamburg-Eppendorf, Hamburg, Germany; the [3]Department of Anatomy and Neurobiology, Washington University School of Medicine, St. Louis, Missouri; and the [5]Division of Pediatric Respiratory Sciences, Johns Hopkins Children's Center, Johns Hopkins Medical Institutions, Baltimore, Maryland.

Supported by grants from the National Institutes of Health (NIH EY015523 and EY019874 to ASJ, and EY001765 to Wilmer Microscopy Core Facility), Medical Illness Counseling Center, The J. Willard and Alice S. Marriott Foundation (both to ASJ), Research to Prevent Blindness (to Wilmer Eye Institute), and the German Research Foundation (DFG, MA 5110/2-1 to MM).

Submitted for publication September 24, 2012; revised January 19, 2013; accepted February 8, 2013.

Disclosure: **H. Meng**, None; **M. Matthaei**, None; **N. Ramanan**, None; **R. Grebe**, None; **S. Chakravarti**, None; **C.L. Speck**, None; **M. Kimos**, None; **N. Vij**, None; **C.G. Eberhart**, None; **A.S. Jun**, None

Corresponding author: Albert S. Jun, Wilmer Eye Institute, 400 N. Broadway, Smith Building, Room 5011, Baltimore, MD 21231; aljun@jhmi.edu.

The UPR can activate several pathways to reduce ER stress and clear misfolded proteins. Proteins can be ubiquitinated and signaled for ER-associated proteasomal degradation, whereas larger protein complexes and organelles undergo bulk degradation via macroautophagy.[17] UPR-associated autophagy has been shown to have a critical role in the pathogenesis of many neurodegenerative disorders involving misfolded proteins, including Alzheimer, Parkinson, and Huntington diseases.[18–20]

In our study, we sought to characterize the endothelial phenotype of a novel *Col8a2*$^{L450W/L450W}$ knock-in mouse model of FECD, to compare this phenotype to that of a previously reported *Col8a2*$^{Q455K/Q455K}$ mouse model of FECD, and to study the possible role of autophagy in the pathogenesis of FECD in these two mouse models and human FECD patient specimens.

Materials and Methods

Transgenic Mouse

Animal use was approved by the Johns Hopkins Animal Care and Use Committee, and adhered to the ARVO Statement for the Use of Animals in Ophthalmic and Vision Research. *Col8a2*$^{L450W/L450W}$ knock-in mice were generated as described previously.[16] In brief, a T-to-G transversion producing a leucine-to-tryptophan substitution at amino acid 456 was introduced into the *Col8a2* gene on mouse chromosome 4. This mutation is homologous to the L450W FECD mutation in the human *COL8A2* gene. The L450W mutation (underlined) in the *Col8a2* targeting vector was produced by overlap extension PCR mutagenesis using overlap primers: L450W-F (5′-GACAGAAAGGTGACTGGGGGCTTCCTGGG-3′) and L450W-R (5′-CCCAGGAAGCCCCCAGTCACCTTTCTGTC-3′). Chimeric animals were bred with C57/BL6J mice, and Southern blotting and DNA sequencing were used to confirm the presence of one copy of the L450W mutation (Figs. 1A, 1B). Heterozygous offspring then were bred to produce mice homozygous for the L450W mutation. *Col8a2*$^{L450W/L450W}$ knock-in mice then were crossed with cre-recombinase expressing Tg(Sox2-cre)1Amc/J mice (stock No. 4783; Jackson Labs, Bar Harbor, ME; kindly provided by Jeremy Nathans, MD, PhD) to excise the pGK-neomycin cassette. Sequence analysis confirmed the absence of any additional mutations within the amino acid coding and intervening intronic regions of *Col8a2,* and also confirmed proper excision of the pGK-neomycin cassette. Wild-type (WT) mice, *Col8a2*$^{L450W/L450W}$ mutant mice (L450W), and *Col8a2*$^{Q455K/Q455K}$ mutant mice (Q455K, described previously[16]) were used for subsequent studies at the indicated ages.

Genotyping

DNA was extracted from mouse tails using the DNeasy Blood and Tissue Kit (Qiagen, Valencia, CA). Genotyping for *Col8a2*^{L450W} mutants was performed by PCR amplification of the *Col8a2* gene using the following primers: forward primer 5′- ATTCGAGGAGACCAAGGGCC-TAAT –3′ and reverse primer 5′- AAGTGAGCACTGCAGTAAAGGCTG –3′. PCR products were cleaned using the GeneJET PCR Purification Kit (Fermentas, Glen Burnie, MD). On gel electrophoresis, L450W homozygous mutant animals have a 269 base pair (bp) fragment post *Bsr*I (New England BioLabs, Ipswitch, MA) restriction enzyme digestion versus a 348 bp fragment for WT animals (Fig. 1C). Genotyping of Q455K homozygous mutant samples was performed as described previously.[16] Clipped tails from WT, *Col8a2*$^{L450W/L450W}$, and *Col8a2*$^{Q455K/Q455K}$ mice also were sent for automated genotyping (Transnetyx, Cordova, TN) using the same forward and reverse primers listed above.

Clinical Confocal Microscopy, Histology, and TEM

These techniques were performed as described previously.[16] TEM was performed on two mice of each age and genotype.

RNA Extraction and Real-Time PCR of Mouse Endothelial Specimens

DM and endothelial cells were stripped from freshly dissected corneas from both eyes of each mouse using the dissection microscope. A total of 4 biological replicates was used for each age and genotype. Total RNA was extracted using the phenol-chloroform method in combination with the RNeasy Micro Kit (Qiagen). After conversion of total RNA to cDNA using the High Capacity RNA-to-cDNA Kit (Life Technologies, Carlsbad, CA), 12.5 μL cDNA were combined with 25 μL TaqMan PreAmp 2x Master Mix (Life Technologies) and 12.5 μL of a custom designed preamplification pool. The custom preamplification pool was created by a 1:100 dilution of each TaqMan assay (Life Technologies) included in the custom TaqMan Array Plate (see Supplementary Material and Supplementary Table S1, http://www.iovs.org/lookup/suppl/doi:10.1167/iovs.12-11021/-/DCSupplemental). A total of 48 μL of amplified products was mixed with 1104 μL nuclease-free water and 1152 μL TaqMan Universal Master Mix II (Life Technologies). Then, 20 μL of the reaction mixture were pipetted in each well of a custom 96-well TaqMan Array Plate (Life Technologies). Real-time PCR array plates were run on a StepOne Plus Real-Time PCR System (Life Technologies).

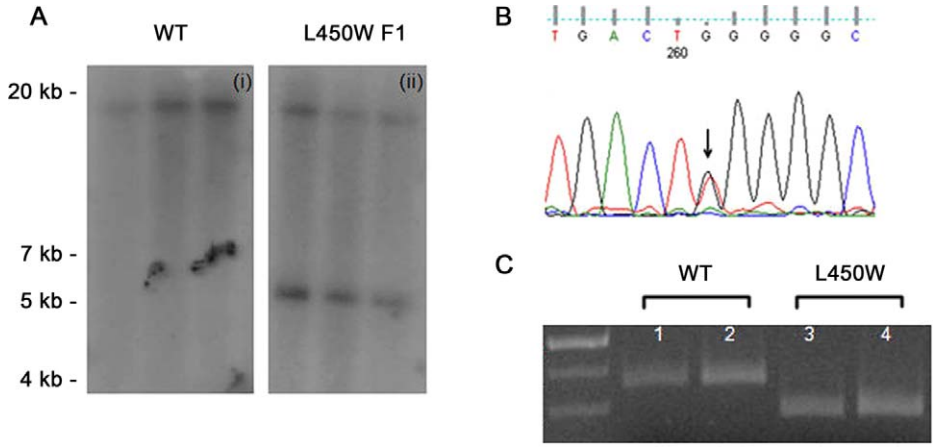

Figure 1. Confirmation of the L450W knock-in mutation**. (A)** Southern blot analysis of WT and L450W mice post *Mfe*I restriction digestion. **(i)** WT animals exhibit a single 18.1 kb band, whereas **(ii)** L450W F1 heterozygous mice have an additional gene-targeted band at 6.1 kb. **(B)** Sequence analysis of the *Col8a2* gene from L450W heterozygous knock-in mice reveals equal levels of T (WT) and G (L450W mutant) bp's by chromatogram signal intensity (*black arrow*). **(C)** *Bsr*I restriction digest of a PCR amplified *Col8a2* fragment reveals a 348 bp band in WT mice (*lanes 1, 2*) and a 269 bp band in mice homozygous for the L450W mutation (*lanes 3, 4*).

Table. Control and Fuchs Dystrophy Patient Information

Sample	Age	Sex	Race	Cause of Death	Death to Preservation Time, h
Control 1	37	F	African American	Intracerebral hemorrhage	3
Control 2	75	F	Caucasian	Hypoxic-ischemic encephalopathy	19
Control 3	42	F	Caucasian	Anoxic encephalopathy	5
Control 4	42	F	Caucasian	Anoxic encephalopathy	5
Control 5	63	M	Caucasian	Anoxic brain injury	11
Control 6	96	F	Caucasian	Cellulitis, abscess of leg	12
Control 7	96	F	Caucasian	Cellulitis, abscess of leg	12
Control 8	57	F	Caucasian	Multiple myeloma	20
Control 9	70	F	African American	Multisystem organ failure	9
Control 10	70	M	Caucasian	Lung cancer	7
Control 11	70	F	African American	Multisystem organ failure	9
Control 12	55	M	Caucasian	Rectal and throat cancer	12
Control 13	65	M	Caucasian	Respiratory failure	5
Control 14	65	M	Caucasian	Respiratory failure	5
Mean age	65				
SD	18				
Fuchs 1	65	F	Caucasian	Fuchs dystrophy	DSAEK
Fuchs 2	59	F	Caucasian	Fuchs dystrophy	DMEK
Fuchs 3	65	M	Caucasian	Fuchs dystrophy	DSAEK
Fuchs 4	67	F	Caucasian	Fuchs dystrophy	DMEK
Fuchs 5	68	M	Caucasian	Fuchs dystrophy	DSAEK
Fuchs 6	64	F	Caucasian	Fuchs dystrophy	DSAEK
Fuchs 7	73	M	Caucasian	Fuchs dystrophy	DSAEK
Fuchs 8	71	M	Caucasian	Fuchs dystrophy	DSAEK
Fuchs 9	75	M	Caucasian	Fuchs dystrophy	DSAEK
Fuchs 10	71	F	Caucasian	Fuchs dystrophy	DSAEK
Fuchs 11	57	M	Caucasian	Fuchs dystrophy	DMEK
Fuchs 12	91	F	Caucasian	Fuchs dystrophy	DSAEK
Fuchs 13	66	M	Caucasian	Fuchs dystrophy	DSAEK
Mean age	69				
SD	8				

DSAEK, DM stripping automated endothelial keratoplasty; DMEK, DM endothelial keratoplasty.

Please see Supplementary Table S1 (see Supplementary Material and Supplementary Table S1, http://www.iovs.org/lookup/suppl/doi:10.1167/iovs.12-11021/-/DCSupplemental) for full details of TaqMan assays included on the array plate. Expression levels of target genes were normalized to levels of β-actin mRNA expression and analyzed by the delta-delta C_T method ($2^{-\Delta\Delta CT}$) using StepOne v2.1 and Data Assist software (Life Technologies).

RNA Extraction and Real-Time PCR of Human Endothelial Specimens

Use of human endothelial specimens was approved by the Johns Hopkins Institutional Review Board and adhered to the tenets of the Declaration of Helsinki. Corneal scleral buttons obtained from the eye bank (Tissue Bank International, Baltimore, MD; Indiana Lions Eyebank, Indianapolis, IN; and Lions VisionGift, Portland, OR) or kindly provided by Shannath Merbs, MD, PhD, or whole eyes obtained from the Johns Hopkins Pathology Department Autopsy Service (see Table) were used as controls. DMs and endothelial cells were stripped, and immediately suspended in TRIzol solution (Life Technologies) before RNA extraction. FECD specimens were obtained from patients undergoing surgical intervention (see Table). Written informed consent was obtained from all patients. Postsurgery, half of the removed patient endothelium was collected in a 1.5 mL microcentrifuge tube. Control and FECD samples were phenol-chloroform extracted, and the resulting RNA was cleaned using the RNeasy Micro Kit (Qiagen). Total RNA then was converted to cDNA, and 5 μL of the resulting cDNA product were amplified as described above using a preamplification pool with the following TaqMan assays (Life Technologies) in a 1:100 dilution: *DRAM1* (Hs00218048_m1), *TMEM74* (Hs01864854_s1), *MTOR* (Hs_00,234,508_m1), and *ACTB* (Hs99999903_m1). The amplified product was diluted 1:12.5 with nuclease-free water, and 9 μL of the diluted cDNA were mixed with 10 uL TaqMan Universal Master Mix II (Life Technologies) and 1 μL undiluted TaqMan assay (Life Technologies). Real-time PCR was performed using the StepOne Plus Real-Time PCR System (Life Technologies). A total of 3 technical replicates was performed for each sample and gene. Relative expression of *DRAM1*, *TMEM74*, and *MTOR* was calculated as above.

Western Blotting

DM and endothelial cells were stripped off freshly dissected corneas and homogenized in Tissue Protein Extract Reagent (Thermo Fisher Scientific, Rockford, IL) supplemented with 1% protease inhibitor cocktail (Sigma, St. Louis, MO), 1 PhosSTOP Phosphatase Inhibitor Cocktail Tablet (Roche, Mannheim, Germany), and 1% EDTA (Sigma). All protein samples consisted of 2 corneas from the same animal; however, due to low abundance of LC3A/B, pooling of 6 corneas from 3 different mice of the same genotype and age was necessary for that particular target. MCF7 cell extracts (sc-2206; Santa Cruz Biotechnology, Santa Cruz, CA) were used as side-by-side positive controls for UPR markers, BiP (GRP78), and GADD153 (CHOP). Hela cell extracts (ab29545; Abcam, Cambridge, MA) were used as a positive control for LC3A/B. Samples were centrifuged at 12,000*g* for 10 minutes at 4°C and the protein concentration of the supernatant was quantified using the Pierce Bicinchoninic Acid Protein Kit (Thermo Fisher Scientific). Equal aliquots of protein were mixed with 4× NuPage loading dye (Life Technologies) with 2-mercaptoethanol (Sigma) and heated for 5 minutes. Samples then were loaded into a 4% to 20% Mini-PROTEAN TGX Gel (BioRad, Hercules, CA) and subjected to SDS-PAGE separation

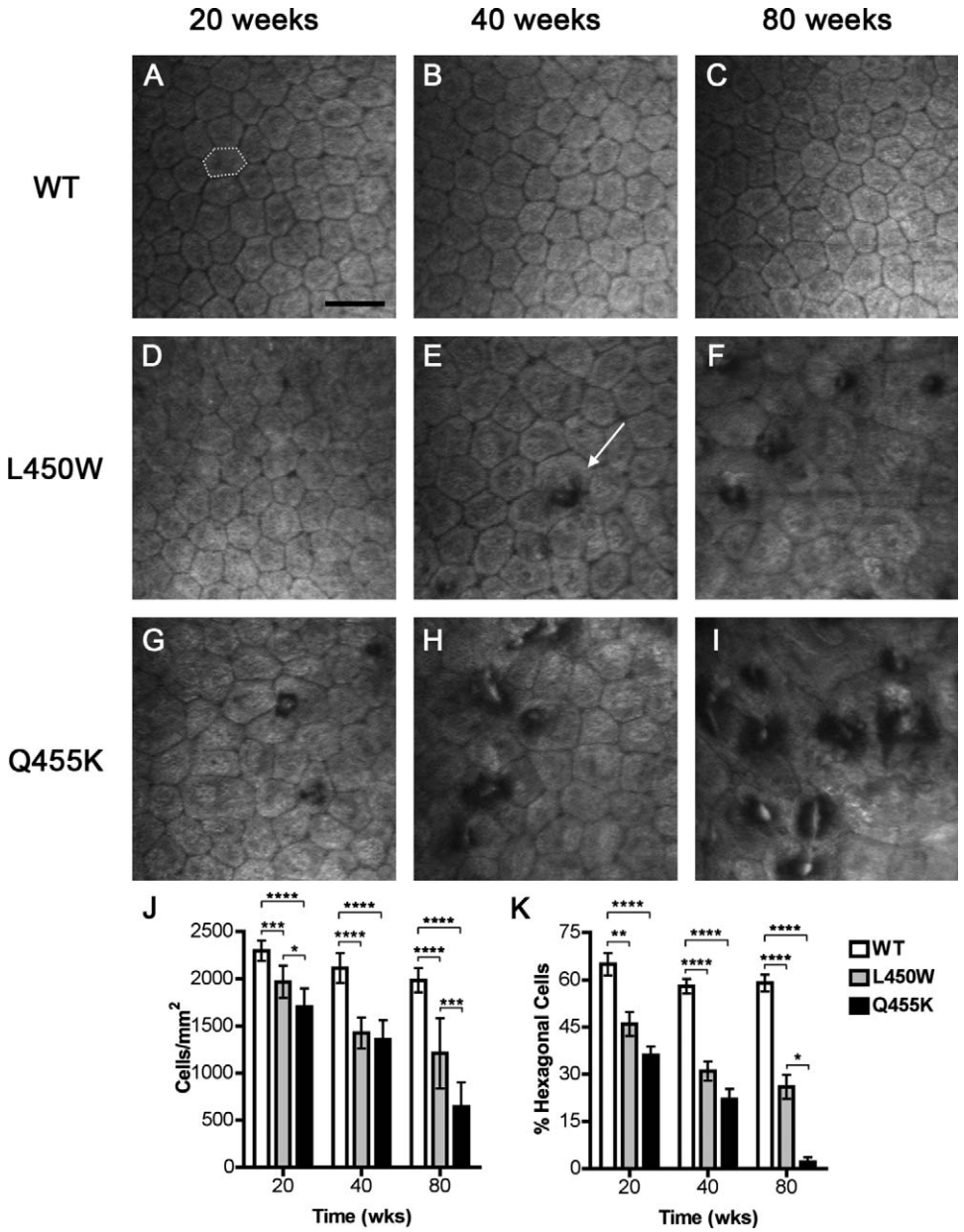

Figure 2. Assessment of corneal endothelium by clinical confocal microscopy. (**A–C**) Images from WT mice at 20, 40, and 80 weeks. *Dotted outline* indicates normal hexagonal shape. (**D–F**) Images from *Col8a2*$^{L450W/L450W}$ mice at 20, 40, and 80 weeks. *Arrow* indicates endothelial gutta. (**G–I**) Images from *Col8a2*$^{Q455K/Q455K}$ mice at 20, 40, and 80 weeks. (**J**) Quantification of cell density with age (weeks). (**K**) Quantification of percent hexagonal cells with age. $^{*}P < 0.05$, $^{**}P < 0.01$, $^{***}P < 0.001$, $^{****}P < 0.0001$. *Scale bar*: 30 μm.

for 30 minutes at 200 V. Proteins were transferred to a polyvinylidene fluoride (PVDF) membrane and incubated in SuperBlock Blocking Buffer (Thermo Fisher Scientific) for 1 hour. Membranes then were incubated in primary antibodies: BiP (1:500, #3183; Cell Signaling, Danvers, MA), GADD153 (1:1000, sc-793; Santa Cruz Biotechnology), LC3A/B (1:500, #4108; Cell Signaling), ATG12 (1:500, #2011; Cell Signaling), and COL8A2 (1:2000; courtesy of Paul Davis, PhD, Wellington, NZ) diluted in blocking buffer for 1 hour at room temperature. Details regarding secondary antibody, membrane stripping, β-actin loading controls, and densitometry analysis are as described previously.[16] Low abundance proteins were detected using SuperSignal West Dura (Thermo Fisher Scientific), and higher abundance proteins were detected using HyGlo Quick Spray (Denville Scientific, Metuchen, NJ).

Statistical Analysis

Statistical significance was determined by unpaired, two-tailed, *t*-tests using PRISM 4 (GraphPad Software, La Jolla, CA). *P* values less than 0.05 were considered statistically significant. All bar graphs show mean ± SEM.

Results

Generation and Corneal Endothelial Characterization of a Novel *Col8a2* L450W Knock-In Mouse Model of FECD

In addition to our previously reported *Col8a2*$^{Q455K/Q455K}$ knock-in mouse model of FECD (Figs. 2G–I),[16] we report here a novel knock-in mouse harboring a T-to-G transversion

resulting in a leucine-to-tryptophan substitution at amino acid 456 in the triple helical domain of the Col8a2 protein. This mutation is homologous to the *COL8A2* L450W mutation observed in genetic studies of FECD.[21]

Southern blotting and *Col8a2* sequence analysis confirmed the correct targeting event, and the presence of the L450W mutation in F1 heterozygotes (Figs. 1A, 1B). Homozygous *Col8a2*$^{L450W/L450W}$ mice exhibited no abnormalities in breeding, behavior, and development; however, upon clinical examination of their corneas, hallmarks of FECD-reduced endothelial cells, guttae, polymegathism (variations in cell size), and pleomorphism (deviations from normal hexagonal shape) were clearly evident (Figs. 2E, 2F).

Col8a2$^{L450W/L450W}$ Mice Exhibit a Less Severe Corneal Endothelial Phenotype Compared to *Col8a2*$^{Q455K/Q455K}$ Mice

Imaging of WT CECs by clinical confocal microscopy revealed an orderly array of endothelial cells, uniform in size and shape, at 20, 40, and 80 weeks (Figs. 2A–C). CECs from 20-week-old WT animals had a CEC density of 2296 ± 106 (mean ± SEM) cells/mm^2 ($n = 8$). At 40 weeks, CEC density dropped to 2115 ± 157 cells/mm^2 ($n = 12$) and, finally, at 80 weeks 1986 ± 128 cells/mm^2 remained ($n = 11$). The decline in CEC density in WT animals is consistent with normal endothelial cell aging in mice.[9]

Col8a2$^{L450W/L450W}$ and *Col8a2*$^{Q455K/Q455K}$ mice at 20, 40, and 80 weeks showed statistically significant decreases in cell density compared to age-matched WT controls (Fig. 2J). The 20-week-old L450W mutant mice exhibited a cell density of 1968 ± 172 cells/mm^2 ($n = 7$) or 14% fewer cells than age-matched WT mice. The 40-week-old *Col8a2*$^{L450W/L450W}$ mice had 1425 ± 165 cells/mm^2 ($n = 13$) or 33% fewer cells than age-matched WT mice. The 80-week-old *Col8a2*$^{L450W/L450W}$ mice had 1209 ± 373 cells/mm^2 ($n = 10$) or 39% fewer cells than age-matched WT mice. In comparison with *Col8a2*$^{L450W/L450W}$ mice, *Col8a2*$^{Q455K/Q455K}$ mice had an earlier onset of guttae and 13% fewer cells at 20 weeks. The 20-week old *Col8a2*$^{Q455K/Q455K}$ mice had 1706 ± 191 cells/mm^2 ($n = 6$) or 26% less cells than age-matched WT mice. The 40-week-old *Col8a2*$^{Q455K/Q455K}$ mice had 1358 ± 202 cells/mm^2 ($n = 15$) or 36% fewer cells than age-matched WT mice. The 80-week-old *Col8a2*$^{Q455K/Q455K}$ mice had 643 ± 258 cells/mm^2 ($n = 11$) or 68% fewer cells than age-matched WT mice. There was a profound difference in cell number between *Col8a2*$^{Q455K/Q455K}$ and *Col8a2*$^{L450W/L450W}$ mice at 80 weeks, with the former having 47% fewer cells than the latter.

Despite a slowly progressive decline in cell density, guttae were seen rarely in WT endothelial images, and CECs maintained a consistent hexagonal shape (dotted outline in Fig. 2A). In WT mice at 20, 40, and 80 weeks, 65 ± 10%, 58 ± 8%, and 59 ± 9% of the cells, respectively, exhibited the normal hexagonal morphology (Figs. 2A–C, 2K). In contrast, 20 week-old *Col8a2*$^{L450W/L450W}$ and *Col8a2*$^{Q455K/Q455K}$ mice had few guttae (Figs. 2D, 2G) and morphologic changes were observed in both mutant mice (Fig. 2K), with 46 ± 10% of the CECs in *Col8a2*$^{L450W/L450W}$ and 36 ± 7% of *Col8a2*$^{Q455K/Q455K}$ mice exhibiting the characteristic hexagonal shape. By 40 weeks, more guttae were observed in both mutant knock-in lines (Figs. 2E, 2H), and the number of hexagonal CECs declined to 31 ± 11% and 22 ± 13% in *Col8a2*$^{L450W/L450W}$ and *Col8a2*$^{Q455K/Q455K}$ mice, respectively (Fig. 2K). By 80 weeks, 26 ± 12% of the CECs maintained hexagonality in the *Col8a2*$^{L450W/L450W}$ mice, whereas, *Col8a2*$^{Q455K/Q455K}$ mice had very few hexagonal cells remaining, with just 2 ± 5% of cells maintaining normal size and shape (Fig. 2K). Overall, *Col8a2*$^{Q455K/Q455K}$ mice had a more severe FECD-like disease phenotype compared to *Col8a2*$^{L450W/L450W}$ mice. More guttae were observed in *Col8a2*$^{Q455K/Q455K}$ mice at each time point, *Col8a2*$^{Q455K/Q455K}$ mice had approximately 50% fewer endothelial cells at 80 weeks of age, and of the remaining cells at 80 weeks, 92% fewer exhibited the normal hexagonal shape.

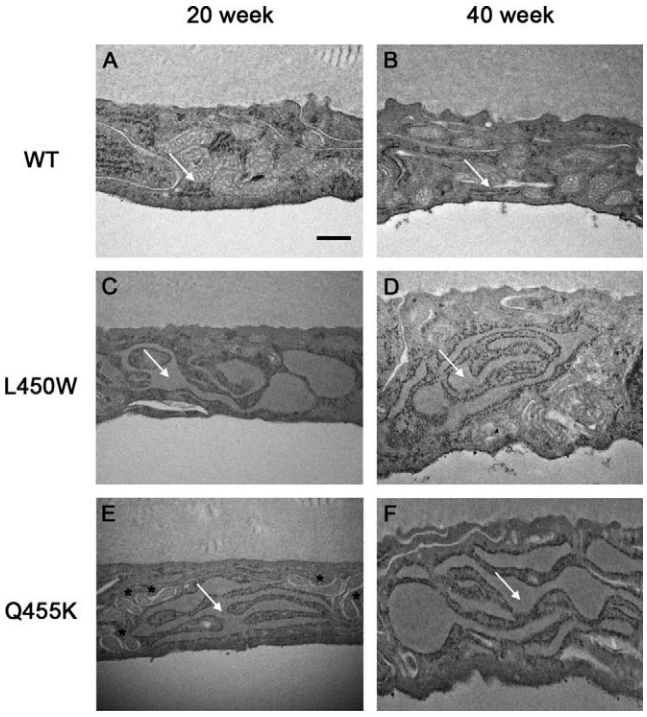

Figure 4. TEM of 20- and 40-week-old *Col8a2*$^{L450W/L450W}$ and *Col8a2*$^{Q455K/Q455K}$ corneal endothelium reveals dilated RER. (**A**, **B**) Images of WT endothelium reveal abundant mitochondria and normal RER (*white arrows*). (**C**–**F**) Mutant L450W and Q455K animals have dilated RER (*white arrows*). (**E**) The 20-week-old Q455K animals have clusters of degenerated mitochondria (*asterisks*). *Scale bar*: 500 nm for (**A**–**F**).

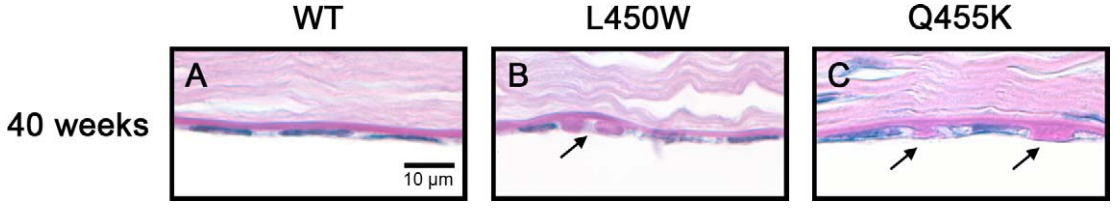

Figure 3. Histologic staining reveals guttae in corneas of 40-week *Col8a2*$^{L450W/L450W}$ and *Col8a2*$^{Q455K/Q455K}$ mice**.** (**B**, **C**) illustrate DM excrescences (*guttae, arrows*) characteristic of FECD.

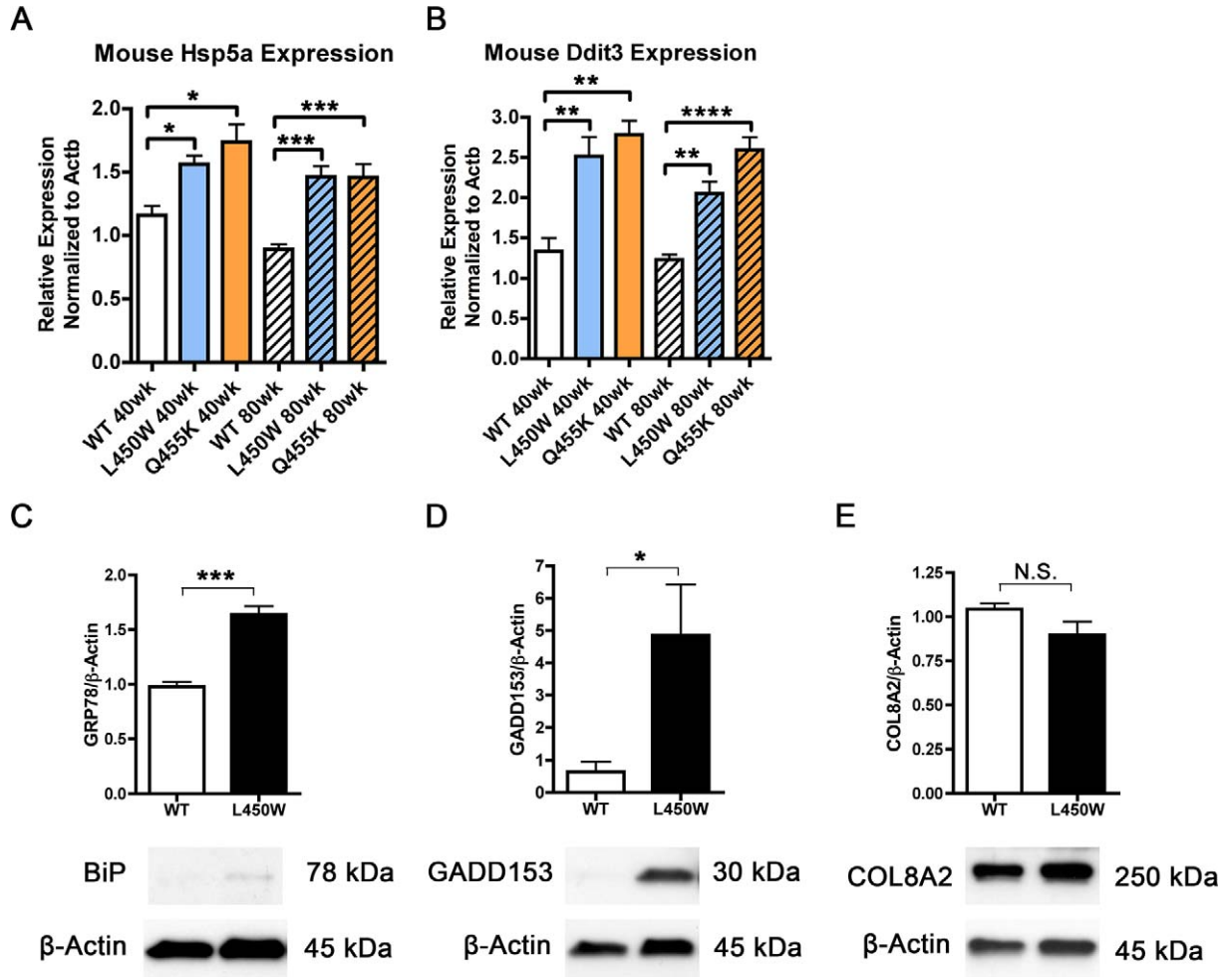

Figure 5. Real-time PCR and Western blotting confirms upregulation of UPR markers in *Col8a2*$^{L450W/L450W}$ and *Col8a2*$^{Q455K/Q455K}$ corneal endothelium. (**A**) Real-time PCR of 40- and 80-week-old mutant mice reveals upregulation of *Hsp5a* (*BiP, Grp78*) compared to age-matched WT control animals. (**B**) Real-time PCR of 40- and 80-week-old mutant mice reveals upregulation of *Ddit3* (*Gadd153*) compared to age-matched WT control animals. (**C**, **D**) Western blotting reveals upregulation of BiP (Grp78) and Gadd153 in 40-week-old *Col8a2*$^{L450W/L450W}$ mice ($n = 5$ for BiP, $n = 4$ for Gadd153) compared to age-matched controls ($n = 5$ for BiP, $n = 3$ for Gadd153). (**E**) Western blotting reveals no difference in Col8a2 protein levels ($n = 3$ for WT and L450W groups). $^{*}P < 0.05$, $^{**}P < 0.01$, $^{***}P < 0.001$, $^{****}P < 0.0001$, N.S., not significant.

Histologic Staining Reveals Guttae in Corneas of *Col8a2*$^{L450W/L450W}$ and *Col8a2*$^{Q455K/Q455K}$ Mice

Overall, corneas of *Col8a2*$^{L450W/L450W}$ and *Col8a2*$^{Q455K/Q455K}$ mice revealed epithelial and stromal features similar to WT mice (not shown), although fewer endothelial cells were observed consistently in both mutant lines. Furthermore, excrescences of DM (Figs. 3B, 3C) also could be observed in mutants (absent in WT, Fig. 3A), which corresponded to the corneal guttae observed by clinical confocal microscopy.

TEM Reveals Dilated RER in *Col8a2*$^{L450W/L450W}$ and *Col8a2*$^{Q455K/Q455K}$ Corneal Endothelium

TEM of WT corneas at 20 and 40 weeks revealed abundant mitochondria and RER with compact lumina (Figs. 4A, 4B). In contrast, TEM of corneas from 20- and 40-week-old *Col8a2*$^{L450W/L450W}$ mice revealed significantly dilated RER (Figs. 4C, 4D). Similarly, dilated RER was observed in 20- and 40-week-old *Col8a2*$^{Q455K/Q455K}$ mice (Figs. 4E, 4F). Abnormal, partially degenerated mitochondria also could be found in 20-week-old *Col8a2*$^{Q455K/Q455K}$ mice (Fig. 4E).

Real-Time PCR and Western Blotting Confirms Upregulation of Unfolded Protein Response Markers in *Col8a2*$^{L450W/L450W}$ and *Col8a2*$^{Q455K/Q455K}$ Corneal Endothelium

Real-time PCR of *Hsp5a* (gene that codes for BiP, a UPR marker) revealed a 1.4-fold and a 1.5-fold upregulation in 40-week-old *Col8a2*$^{L450W/L450W}$ and *Col8a2*$^{Q455K/Q455K}$ mice, respectively, compared to WT mice (Fig. 5A). At 80 weeks of age *Col8a2*$^{L450W/L450W}$ and *Col8a2*$^{Q455K/Q455K}$ mice showed a 1.6-fold and a 1.6-fold upregulation of *Hsp5a* expression, respectively (Fig. 5A). Gene expression of *Ddit3* (gene that codes for UPR marker Gadd153) also was upregulated at 40 weeks, with *Col8a2*$^{L450W/L450W}$ and *Col8a2*$^{Q455K/Q455K}$ mice exhibiting a 1.9-fold and a 2.1-fold upregulation, respectively (Fig. 5B). At 80 weeks of age *Col8a2*$^{L450W/L450W}$ and *Col8a2*$^{Q455K/Q455K}$ mice exhibited a 1.7-fold and a 2.1-fold upregulation, respectively (Fig. 5B). Real-time PCR results were consistent with previously published results reporting upregulation of UPR genes and proteins in *Col8a2*$^{Q455K/Q455K}$ mice.[16] To confirm further upregulation of UPR in *Col8a2*$^{L450W/L450W}$ mice, we quantified BiP and Gadd153 proteins in 40-week-old mutant and WT mice (Figs. 5C–E). *Col8a2*$^{L450W/L450W}$ mice

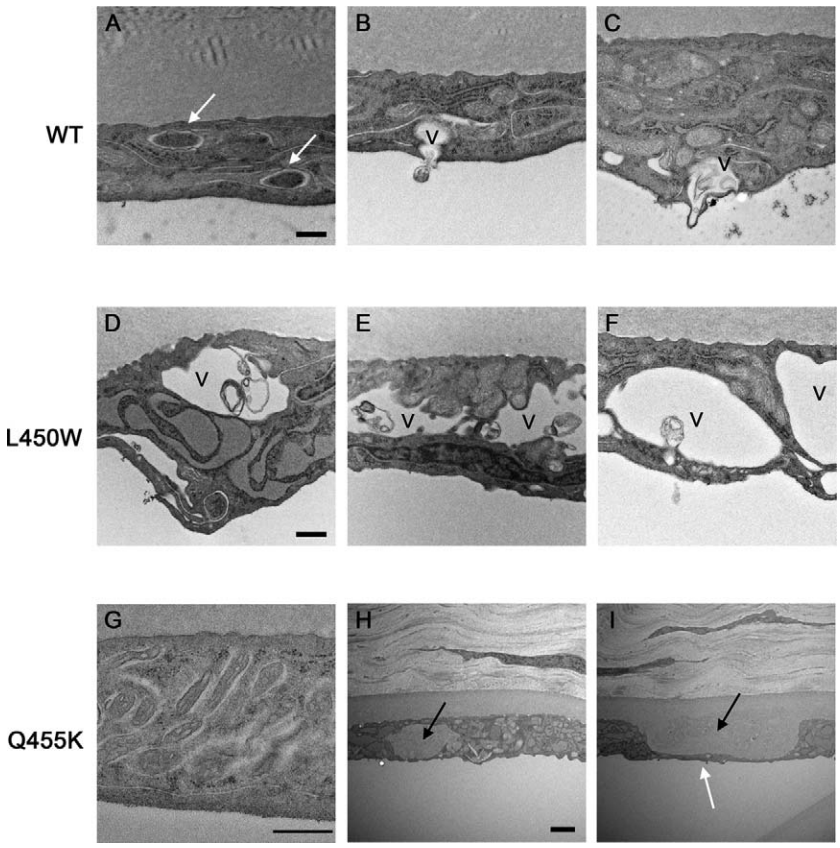

Figure 6. TEM reveals altered degradation processes in *Col8a2*$^{L450W/L450W}$ and *Col8a2*$^{Q455K/Q455K}$ corneal endothelium**.** (**A**) 20-week-old WT mouse endothelial cell with normal autophagosomes (*white arrows*). (**B**) 20-week-old WT and (**C**) 40-week-old WT CECs releasing the contents of a vacuole (labeled '*v*') with partially degraded organelles into the aqueous humor. (**D**, **E**) 20-week old *Col8a2*$^{L450W/L450W}$ mice with abnormal accumulation of mitochondria (**E**) and large electron lucent vacuoles (*v*) containing partially degraded organelles. (**F**) 40-week old *Col8a2*$^{L450W/L450W}$ mouse with large, mostly empty, electron lucent vacuoles (*v*). (**G**) 20-week-old *Col8a2*$^{Q455K/Q455K}$ mice with abnormal accumulation of mitochondria. (**H**) 40-week-old *Col8a2*$^{Q455K/Q455K}$ mouse with a large amorphous region where part of the endothelial cell has degraded (*black arrow*). (**I**) 40-week-old *Col8a2*$^{Q455K/Q455K}$ mouse with the presumed remains of a dead endothelial cell (*black arrow*). Neighboring cells extend appendages to maintain cell-to-cell contact (*white arrow*). *Scale bars*: 500 nm (**A**–**G**); 2 μm (**H**, **I**).

exhibited a 1.7-fold upregulation in BiP and a 7.6-fold upregulation in Gadd153 compared to age-matched WT. Consistent with published results indicating comparable levels of Col8a2 protein in *Col8a2*$^{Q455K/Q455K}$ mice compared to WT,[16] no significant difference was observed in Col8a2 protein levels in *Col8a2*$^{L450W/L450W}$ mice compared to WT.

TEM Reveals Altered Degradation in *Col8a2*$^{L450W/L450W}$ and *Col8a2*$^{Q455K/Q455K}$ Corneal Endothelium

TEM of a 20-week-old WT mouse revealed double-membrane autophagosomes characteristic of normal autophagic processes (Fig. 6A). Both 20- and 40-week-old WT mice also contained vacuoles with partially degraded organelles fusing to the plasma membrane and releasing their contents into the aqueous humor (Figs. 6B, 6C). In comparison with WT animals, *Col8a2*$^{L450W/L450W}$ mice at 20 weeks contained abnormal accumulations of mitochondria and large, electron-lucent vacuoles enclosing partially degraded organelles (Figs. 6D, 6E). The vacuoles increased in size in 40-week-old *Col8a2*$^{L450W/L450W}$ mice, and the majority of vacuoles appeared empty, with the occasional partially degraded organelle remaining (Fig. 6F). Fewer dilated ER could be found in 40-week-old *Col8a2*$^{L450W/L450W}$ mice, and the majority of the cell volume consisted of empty vacuoles. In comparison, 20- and 40-week-old *Col8a2*$^{Q455K/Q455K}$ mice did not exhibit these same electron-lucent vacuoles. The 20-week-old *Col8a2*$^{Q455K/Q455K}$ mice exhibited many abnormal mitochondria (Fig. 6G) and persistently dilated RER at 40 weeks of age (Fig. 4F). Large areas of cellular degradation also could be observed in *Col8a2*$^{Q455K/Q455K}$ mice, which appeared to have a proteinaceous electron density similar to DM (Fig. 6H). When sufficient areas of the endothelial cell had been degraded, apparent fusion with DM occurred (Fig. 6I). Neighboring endothelial cells extended appendages to cover the degraded remains of the dead endothelial cell, thereby maintaining cell-to-cell contact (Fig. 6I).

Real-Time PCR Reveals Upregulation of Autophagy Inducers *Dram1* and *Tmem74* in *Col8a2*$^{L450W/L450W}$ and *Col8a2*$^{Q455K/Q455K}$ Corneal Endothelium

Given that TEM revealed accumulation of large vacuoles with partially degraded organelles and bulk degradation of large portions of endothelial cells, we wanted to investigate autophagy regulation, a key degradation pathway that is triggered by accumulation of misfolded proteins and the unfolded protein response.[22,23] In addition to the analysis of the UPR (Fig. 5), we analyzed the expression of 89 autophagy-related genes in endothelium of mutant and WT mice by real-time PCR (see Supplementary Material and Supplementary

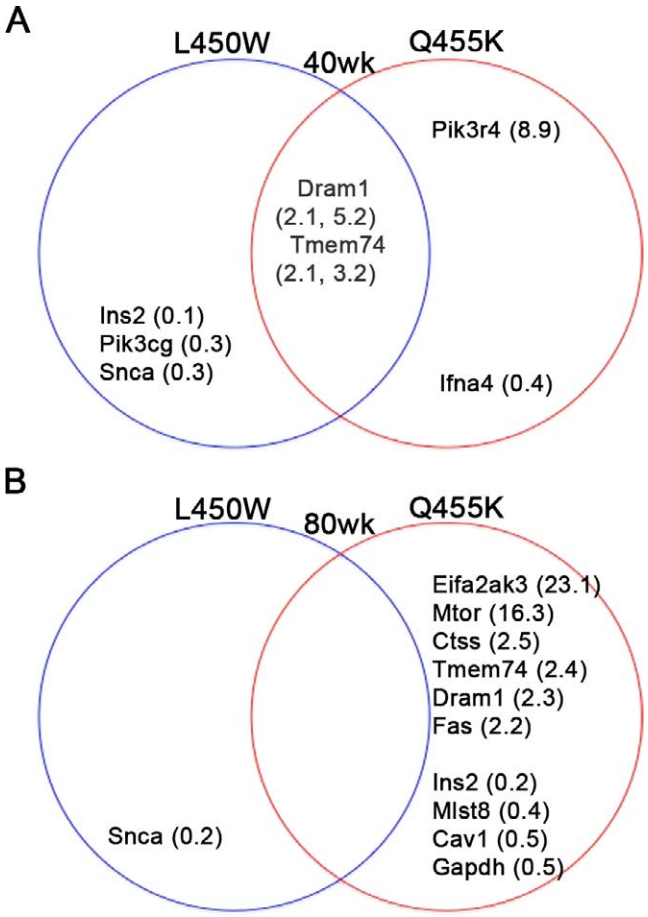

FIGURE 7. Relative expression of autophagy-related genes in *Col8a2*$^{L450W/L450W}$ and *Col8a2*$^{Q455K/Q455K}$ corneal endothelium detected by real-time PCR. (**A**) Relative gene expression ($P < 0.05$) of CECs of 40-week-old *Col8a2*$^{L450W/L450W}$ ($n = 4$) and *Col8a2*$^{Q455K/Q455K}$ mice ($n = 4$). (**B**) Relative gene expression ($P < 0.05$) of CECs of 80-week-old *Col8a2*$^{L450W/L450W}$ ($n = 4$) and *Col8a2*$^{Q455K/Q455K}$ mice ($n = 4$). The intersection of the Venn diagrams shows genes that were upregulated in *Col8a2*$^{L450W/L450W}$ and *Col8a2*$^{Q455K/Q455K}$ mice. Values in parentheses always are listed with *Col8a2*$^{L450W/L450W}$ relative expression values first followed by *Col8a2*$^{Q455K/Q455K}$ expression values. All values are normalized to β-actin and expressed as quantities relative to age-matched WT controls ($n = 4$ per age group).

Table S1, http://www.iovs.org/lookup/suppl/doi:10.1167/iovs.12-11021/-/DCSupplemental). We identified genes that exhibited at least a statistically significant 2-fold up- or down-regulation compared to age-matched WT mice (Figs. 7A, 7B).

At 40 weeks, analysis of *Col8a2*$^{L450W/L450W}$ CECs showed a 2.1-fold increase in expression of DNA-damage regulated autophagy modulator (*Dram1*) and 2.1-fold increase in expression of transmembrane protein 74 (*Tmem74*) compared to age-matched WT CECs (Figs. 7A, 9A, 9B). In the same mice, we also observed a 7.7-fold decrease in insulin II (*Ins2*), a 3.1-fold decrease in phosphoinositide-3-kinase, catalytic subunit gamma (*Pik3cg*), and a 3.0-fold decrease in alpha-synuclein (*Snca*) expression (Fig. 7A). At 80 weeks (Fig. 7B), *Snca* exhibited 5.3-fold lower expression than age-matched WT; however, *Dram1*, *Tmem74*, *Ins2*, and *Pik3cg* no longer exhibited statistically significant differences in expression.

At 40 weeks, CECs from *Col8a2*$^{Q455K/Q455K}$ mice revealed a significant increase in *Dram1* and *Tmem74* by 5.2-fold and 3.2-fold, respectively (Figs. 7A, 9A, 9B). An 8.9-fold increase of phosphoinositide-3-kinase, regulatory subunit 4 (*Pik3r4*) and a 2.6-fold decrease of interferon alpha 4 (*Ifna4*) also was observed. The 80-week-old *Col8a2*$^{Q455K/Q455K}$ CECs exhibited upregulation of the following genes: Eukaryotic translation initiation factor 2-alpha kinase 3 (*Eif2ak3*) by 23.1-fold, mechanistic target of rapamycin (*Mtor*) by 16.3-fold, cathepsin S (*Ctss*) by 2.5-fold, *Tmem74* by 2.4-fold, *Dram1* by 2.3-fold, and tumor necrosis factor receptor superfamily, member 6 (*Fas*) by 2.2-fold (Fig. 7B). Four genes also were down-regulated by greater than 2-fold. Insulin II (*Ins2*) was down-regulated 5.0-fold, Mtor associated protein, Lst8 homolog (*Mlst8*) was down-regulated 2.6-fold, caveolin 1 (*Cav1*) was down-regulated 2.2-fold, and glyceraldehyde-3-phosphate dehydrogenase (*Gapdh*) was down-regulated 2.2-fold (Fig. 7B).

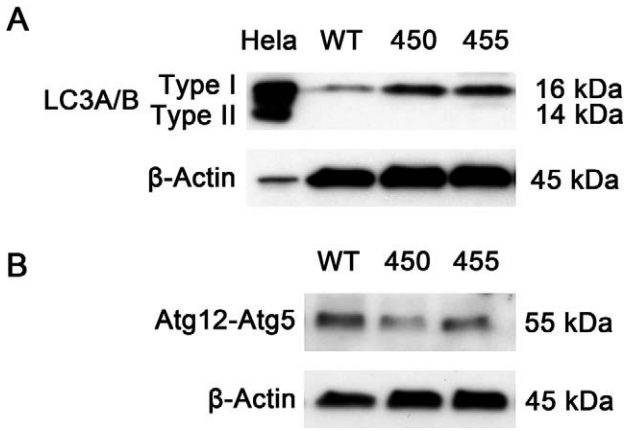

FIGURE 8. Western blotting indicates altered autophagy in *Col8a2*$^{L450W/L450W}$ and *Col8a2*$^{Q455K/Q455K}$ corneal endothelium. (**A**) LC3-I and LC3-II protein levels in 40-week-old WT, *Col8a2*$^{L450W/L450W}$, and *Col8a2*$^{Q455K/Q455K}$ endothelium shows upregulation of LC3-I protein in mutant animals. Proteins loaded in each lane were pooled from 3 mice (6 corneas) of the specified genotype. We analyzed 3 pooled groups per genotype, one representative image is shown here. Hela cell lysate was used as a positive control. (**B**) Conjugated Atg12-Atg5 protein levels in 40-week-old WT ($n = 4$), *Col8a2*$^{L450W/L450W}$ ($n = 4$), and *Col8a2*$^{Q455K/Q455K}$ ($n = 4$) endothelium show decreased levels of Atg12-Atg5 in mutant animals. One representative image is shown here.

LC3A/B and ATG12-5 Protein Analyses Indicate Altered Autophagy in *Col8a2*$^{L450W/L450W}$ and *Col8a2*$^{Q455K/Q455K}$ Corneal Endothelium

Given the upregulation of autophagy regulatory markers, *Dram1* and *Tmem74*, by real-time PCR, we wanted to assess further for upregulation of autophagy by testing for proteins associated with autophagosome formation, LC3 and Atg12 in 40-week-old mutant endothelium. Western blotting using anti-LC3A/B antibody revealed upregulation of LC3-I in mutant endothelium, but no LC3-II bands could be detected (Fig. 8A). Western blotting using anti-Atg12 antibody revealed a decreased abundance of conjugated Atg12-Atg5 in mutant endothelium compared to age-matched controls (Fig. 8B).

Real-Time PCR of Human FECD Endothelium Reveals a 10.4-Fold Upregulation of *DRAM1* Compared to Autopsy Controls

Given evidence for increased macroautophagy by TEM, and gene expression changes in *Dram1* and *Tmem74* in mouse CECs, we wanted to determine whether either of these autophagy-associated genes was upregulated in CECs from human FECD patients. A total of 14 CEC samples was obtained

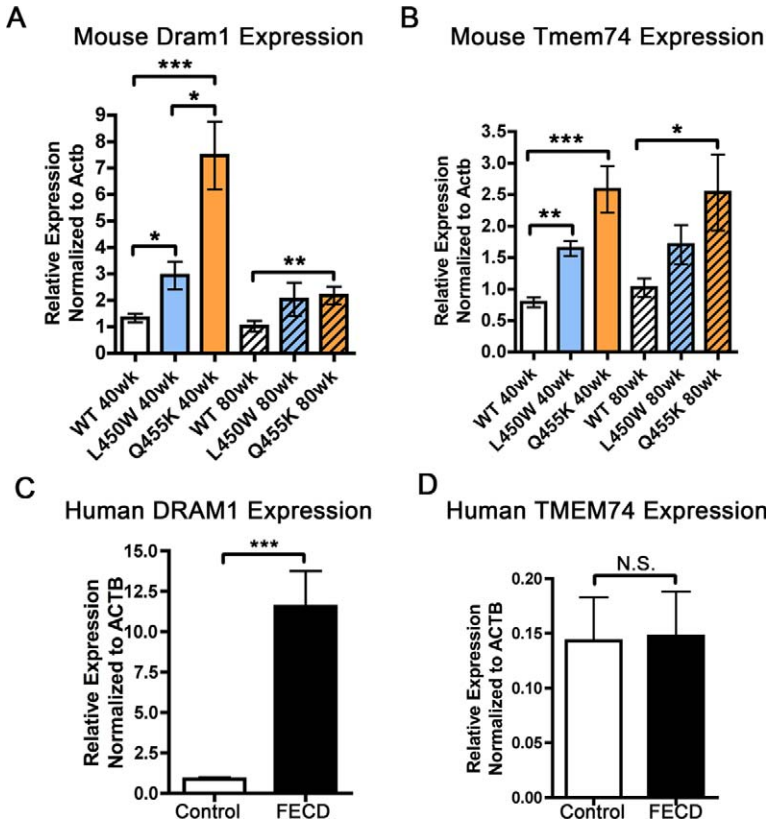

Figure 9. Real-time PCR of mouse and human endothelium reveals upregulation of autophagy regulators. **(A)** Real-time PCR reveals upregulation of *Dram1* in *Col8a2*$^{L450W/L450W}$ and *Col8a2*$^{Q455K/Q455K}$ mice at 40 weeks of age. At 80 weeks of age, *Dram1* is upregulated significantly only in *Col8a2*$^{Q455K/Q455K}$ mice. **(B)** *Tmem74* real-time PCR reveals upregulation in both mutant mice at 40 weeks; however, only 80-week-old *Col8a2*$^{Q455K/Q455K}$ mice exhibit upregulation compared to age-matched WT. Real-time PCR of human endothelium reveals upregulation of *DRAM1* **(C)** and no difference in *TMEM74* **(D)** in FECD samples compared to normal controls. $^{*}P < 0.05$, $^{**}P < 0.01$, $^{***}P < 0.001$.

from autopsy patients or research corneas obtained from the eye bank (see Table). Of the endothelial cell samples 13 were obtained from patients undergoing endothelial transplant due to FECD with unknown genotypes. We extracted whole RNA from each sample, and analyzed *DRAM1*, *TMEM74*, and *MTOR* by real-time PCR. Analysis revealed a 10.4-fold upregulation ($P < 0.0001$) of *DRAM1* in FECD samples compared to control samples (Fig. 9C). However, we found no statistically significant differences in *TMEM74* (Fig. 9D) or *MTOR* expression (not shown).

Discussion

We report the second mouse model of FECD produced by knock-in of the L450W *Col8a2* mutation, which is an allelic variant of the Q455K mutation reported previously by our group.[16] Interestingly, L450W mutant mice show a milder clinical phenotype on confocal microscopy compared to Q455K mice, although this relative preservation of cells and morphology is associated with a seemingly more "severe" vacuolization on TEM. Available clinical information is insufficient to allow detailed comparison of phenotypic severity between human L450W and Q455K patients. Liskova et al. describe a single L450W pedigree, with one patient who underwent penetrating keratoplasty at age 75, and a second who suffered edema in the "mid-20s" and subsequently underwent bilateral keratoplasty in the 30s and 40s.[24] Gottsch et al. describe another L450W pedigree with two patients who underwent keratoplasty in the late 40s and two patients with edema in the 30s.[21] Biswas et al. provide clinical descriptions for two of the three FECD pedigrees they reported as having the Q455K mutation. Pedigree 1 included a patient who had edema in the 30s to 40s, and pedigree 2 included a patient who underwent bilateral keratoplasty in the 50s but had symptoms from edema in the 20s.[10] Thus, the available information suggests that in humans the phenotypes associated with the L450W and Q455K mutations are more similar than observed in mice. Such variation in humans may be more difficult to discern for multiple reasons, including heterogeneity of genetic background/modifier genes as well as the longer time of disease progression. These issues underscore the potential value of using mouse models to define genotype/phenotype relationships in FECD.

Similar to the previously reported Q455K knock-in mouse line,[16] we provided evidence for ER stress and UPR in L450W knock-in mouse corneal endothelium, including marked enlargement of ER and upregulation of UPR markers. Such ER expansion occurred within the cell to lower the concentration of toxic unfolded proteins and reestablish homeostasis.[22] The precise identity of toxic unfolded proteins within the dilated ER is difficult to determine. Western blots of endothelium from both mutant lines showed comparable levels of trimeric Col8a2 with WT, and no increased amounts of monomeric or partial length Col8a2 peptides were observed. However, it remains possible that the accumulated unfolded proteins are comprised of Col8a2 peptide fragments not containing the epitopes recognized by the antibody used. Alternatively, a relatively small subpopulation of defective Col8a2 protein could alter global protein processing/trafficking within the ER resulting in nonspecific protein accumula-

tion. Elegant experiments by Bernales et al. indicate that cells can respond further to extreme levels of toxic unfolded proteins within abnormal regions of ER by sequestering these areas inside large membrane-bound vacuoles.[25] This process involves an organelle-specific form of macroautophagy termed "ER-phagy."[25]

It is tempting to speculate that the expanded ER and large membrane-containing vacuoles represent ER-phagy in the corneal endothelium of L450W mice, which confers increased survival compared to Q455K endothelium lacking these features. Thus, although both mutations occur in close proximity within the protein and appear grossly to induce similar ER stress/UPR activation, we suggested that they could potentially produce allele-specific biochemical defects and downstream cell survival responses. This possibility is supported by our previous studies of these two mutations using circular dichroism spectroscopy and transfection in a cell culture model of FECD.[26]

Macroautophagy is a well-studied cellular pathway that degrades bulk protein aggregates and organelles. Evidence of ER stress and large, organelle-containing vacuoles in L450W corneal endothelium prompted us to investigate markers of autophagy in our two mouse lines and human FECD patients. Custom autophagy gene expression arrays showed upregulation of *Dram1* and *Tmem74 in* L450W and Q455K endothelium at 40 weeks. In addition, *Dram1* was upregulated in endothelium from 80-week Q455K mice and human FECD patients.

Damage-regulated autophagy modulator (DRAM) is required for p53-mediated induction of autophagy and apoptosis.[27] Interestingly, *Dram1* upregulation in our study remained elevated in 80-week mice only for the more severely affected Q455K line, which presumably had higher levels of endothelial cell apoptosis. Our findings supported the previous work by Azizi et al. who showed that p53-mediated apoptosis has an important role in FECD.[28] Furthermore, these results suggested that, in addition to established oxidative stress pathways, autophagy and *DRAM1* contribute to p53-mediated apoptosis of corneal endothelium in Q455K mice and human FECD patients.

The role of transmembrane protein (Tmem) 74 is less clear as its expression was not elevated in 80-week-old L450W mice or FECD patients. Available reports of this protein are limited and indicate that it functions as an autophagy inducer.[29,30] Further study may reveal alternative activities for *Tmem74*, which may explain the apparent inconsistency we observed between its expression and *Dram1* in our mouse models and human patients.

Although we observed increased levels of LC3-I in the corneal endothelium of both mouse models, we did not observe upregulation of LC3-II, a common marker of autophagy. Given the limited amount of protein that we were able to extract from mouse corneas and the technical demands of isolating intact LC3-II, we may not have obtained sufficient protein to detect lower abundance LC3-II. In addition, cells of neuronal origin, including corneal endothelium,[31,32] may show a low ratio of LC3-II to LC3-I due to rapid LC3-II degradation.[33]

The finding of decreased ATG12-5 and abnormal accumulations of mitochondria in corneal endothelium from both mutant mouse lines is comparable to the results of Luo et al., who noted decreased ATG12-5, increased mitochondria, and decreased DJ-1 protein in cardiomyocytes exposed to *tert*-butyl hydroperoxide (tBHP)–induced oxidative stress.[34] These investigators concluded that defects in autophagy resulted in decreased organelle turnover leading to mitochondrial accumulation. Interestingly, Bitar et al. noted decreased DJ-1 and other Nrf2-related proteins in tBHP exposed corneal endothelium from FECD patients.[35] Thus, it is possible that altered autophagy in FECD patient endothelium also contributes to the observed decrease in DJ-1.

Our findings confirmed the sufficiency of the L450W and Q455K COL8A2 mutations to cause early-onset FECD in humans, and they further underscored the potential to model corneal endothelial diseases accurately in mice. This approach indicated a role for altered autophagy at an earlier clinical stage than has been studied in humans. The use of an in vivo model associated with a rare and phenotypically distinct form of FECD may limit its applicability to more common forms of the disease. However, our confirmation of elevated *DRAM1* levels in human later onset FECD endothelium with unknown genotypes suggested a pathogenic interaction between autophagy, oxidative stress, and p53 activation, as well as possible therapeutic approaches related to these processes. The development of additional mouse models of FECD using other causative mutations should provide information regarding early cellular pathogenesis that is impractical to obtain in human patients, and that may be valuable for the development and testing of potential nonsurgical treatments for this disease.

Acknowledgments

The authors thank Barbara Crain, MD, PhD, and the Johns Hopkins Pathology Autopsy Service for the autopsy eyes used in this study; Paul Davis, MD, David Ginty, PhD, and Jeremy Nathans, MD, PhD, for technical assistance; and Stanley Friedler, MD, Diane Kemker, Jean Mattison, and Lee Silverman for assistance with funding support.

References

1. Suh LH, Emerson MV, Jun AS. *Cornea and External Eye Disease*. 1st ed. Heidelberg, Germany: Springer; 2008.
2. Van Meter WS. 2009 Eye Banking Statistical Report. http://www.corneas.org/repository/images/pressimages/EBAA%202009%20Statistical%20Report%20-%20Final.pdf. Published 2009. Accessed April 30, 2012.
3. Baratz KH, Tosakulwong N, Ryu E, et al. E2-2 Protein and Fuchs's corneal dystrophy. *New Engl J Med*. 2010;363:1016–1024.
4. Levy SG, Moss J, Sawada H, Dopping-Hepenstal PJ, McCartney AC. The composition of wide-spaced collagen in normal and diseased Descemet's membrane. *Curr Eye Res*. 1996;15:45–52.
5. Zhu YT, Hayashida Y, Kherikhah A, He H, Cheng SY, Tseng SC. Characterization and comparison of intercellular adherent junctions expressed by human corneal endothelial cells in vivo and in vitro. *Invest Ophthalmol Vis Sci*. 2008;49:3879–3886.
6. Joyce NC, Navon SE, Roy S, Zieske JD. Expression of cell cycle-associated proteins in human and rabbit corneal endothelium in situ. *Invest Ophthalmol Vis Sci*. 1996;37:1566–1575.
7. Bourne WM. Biology of the corneal endothelium in health and disease. *Eye (Lond)*. 2003;17:912–918.
8. Bourne WM, Nelson LR, Hodge DO. Central corneal endothelial cell changes over a ten-year period. *Invest Ophthalmol Vis Sci*. 1997;38:779–782.
9. Jun AS, Chakravarti S, Edelhauser HF, Kimos M. Aging changes of mouse corneal endothelium and Descemet's membrane. *Exp Eye Res*. 2006;83:890–896.
10. Biswas S, Munier FL, Yardley J, et al. Missense mutations in COL8A2, the gene encoding the alpha2 chain of type VIII collagen, cause two forms of corneal endothelial dystrophy. *Hum Mol Genet*. 2001;10:2415–2423.
11. Gottsch JD, Zhang C, Sundin OH, Bell WR, Stark WJ, Green WR. Fuchs corneal dystrophy: aberrant collagen distribution in an L450W mutant of the COL8A2 gene. *Invest Ophthalmol Vis Sci*. 2005;46:4504–4511.

12. Mok JW, Kim HS, Joo CK. Q455V mutation in COL8A2 is associated with Fuchs' corneal dystrophy in Korean patients. *Eye (Lond)*. 2009;23:895–903.
13. Engler C, Kelliher C, Spitze AR, Speck CL, Eberhart CG, Jun AS. Unfolded protein response in Fuchs endothelial corneal dystrophy: a unifying pathogenic pathway? *Am J Ophthalmol*. 2010;149:194–202.e2.
14. Zhang C, Bell WR, Sundin OH, et al. Immunohistochemistry and electron microscopy of early-onset Fuchs corneal dystrophy in three cases with the same L450W COL8A2 mutation. *Trans Am Ophthalmol Soc*. 2006;104:85–97.
15. Vithana EN, Morgan PE, Ramprasad V, et al. SLC4A11 mutations in Fuchs endothelial corneal dystrophy. *Hum Mol Genet*. 2008;17:656–666.
16. Jun AS, Meng H, Ramanan N, et al. An alpha 2 collagen VIII transgenic knock-in mouse model of Fuchs endothelial corneal dystrophy shows early endothelial cell unfolded protein response and apoptosis. *Hum Mol Genet*. 2012;21:384–393.
17. Rubinsztein DC, DiFiglia M, Heintz N, et al. Autophagy and its possible roles in nervous system diseases, damage and repair. *Autophagy*. 2005;1:11–22.
18. Bellucci A, Navarria L, Zaltieri M, et al. Induction of the unfolded protein response by alpha-synuclein in experimental models of Parkinson's disease. *J Neurochem*. 2011;116:588–605.
19. Nijholt DA, de Graaf TR, van Haastert ES, et al. Endoplasmic reticulum stress activates autophagy but not the proteasome in neuronal cells: implications for Alzheimer's disease. *Cell Death Differ*. 2011;18:1071–1081.
20. Vidal R, Caballero B, Couve A, Hetz C. Converging pathways in the occurrence of endoplasmic reticulum (ER) stress in Huntington's disease. *Curr Mol Med*. 2011;11:1–12.
21. Gottsch JD, Sundin OH, Liu SH, et al. Inheritance of a novel COL8A2 mutation defines a distinct early-onset subtype of Fuchs corneal dystrophy. *Invest Ophthalmol Vis Sci*. 2005;46:1934–1939.
22. Bernales S, McDonald KL, Walter P. Autophagy counterbalances endoplasmic reticulum expansion during the unfolded protein response. *PLoS Biol*. 2006;4:e423.
23. Ogata M, Hino S, Saito A, et al. Autophagy is activated for cell survival after endoplasmic reticulum stress. *Mol Cell Biol*. 2006;26:9220–9231.
24. Liskova P, Prescott Q, Bhattacharya SS, Tuft SJ. British family with early-onset Fuchs' endothelial corneal dystrophy associated with *p*.L450W mutation in the COL8A2 gene. *Br J Ophthalmol*. 2007;91:1717–1718.
25. Bernales S, Schuck S, Walter P. ER-phagy: selective autophagy of the endoplasmic reticulum. *Autophagy*. 2007;3:285–287.
26. Kelliher C, Chakravarti S, Vij N, et al. A cellular model for the investigation of Fuchs' endothelial corneal dystrophy. *Exp Eye Res*. 2011;93:880–888.
27. Crighton D, Wilkinson S, O'Prey J, et al. DRAM, a p53-induced modulator of autophagy, is critical for apoptosis. *Cell*. 2006;126:121–134.
28. Azizi B, Ziaei A, Fuchsluger T, Schmedt T, Chen Y, Jurkunas UV. p53-regulated increase in oxidative-stress-induced apoptosis in Fuchs endothelial corneal dystrophy: a native tissue model. *Invest Ophthalmol Vis Sci*. 2011;52:9291–9297.
29. He P, Peng Z, Luo Y, et al. High-throughput functional screening for autophagy-related genes and identification of TM9SF1 as an autophagosome-inducing gene. *Autophagy*. 2009;5:52–60.
30. Yu C, Wang L, Lv B, et al. TMEM74, a lysosome and autophagosome protein, regulates autophagy. *Biochem Biophys Res Commun*. 2008;369:622–629.
31. Adamis AP, Molnar ML, Tripathi BJ, Emmerson MS, Stefansson K, Tripathi RC. Neuronal-specific enolase in human corneal endothelium and posterior keratocytes. *Exp Eye Res*. 1985;41:665–668.
32. Hayashi K, Sueishi K, Tanaka K, Inomata H. Immunohistochemical evidence of the origin of human corneal endothelial cells and keratocytes. *Graefes Arch Clin Exp Ophthalmol*. 1986;224:452–456.
33. Klionsky DJ, Abdalla FC, Abeliovich H, et al. Guidelines for the use and interpretation of assays for monitoring autophagy. *Autophagy*. 2012;8:445–544.
34. Luo C, Li Y, Wang H, Feng Z, Long J, Liu J. Mitochondrial accumulation under oxidative stress is due to defects in autophagy. *J Cell Biochem*. 2012;114:212–219.
35. Bitar MS, Liu C, Ziaei A, Chen Y, Schmedt T, Jurkunas UV. Decline in DJ-1 and decreased nuclear translocation of Nrf2 in Fuchs endothelial corneal dystrophy. *Invest Ophthalmol Vis Sci*. 2012;53:5806–5813.